

# Digital hologram recording and stereo reconstruction from a single hologram

Angelo Arrifano<sup>\*†</sup> and Marc Antonini<sup>\*</sup> and Paulo T. Fiadeiro<sup>‡</sup> and Manuela Pereira<sup>†</sup>

<sup>\*</sup>I3S laboratory, University of Nice - Sophia Antipolis / CNRS, France;

<sup>‡</sup>Instituto de Telecomunicacoes, Universidade da Beira Interior, Portugal;

<sup>†</sup>Unidade de Detecção Remota e Centro de Óptica, Universidade da Beira Interior, Portugal

## ABSTRACT

In this paper we present novel results on the reconstruction of stereoscopic information from a single phase-shift hologram captured using a  $2.2\ \mu\text{m}$  pixel-pitch CMOS camera in a holographic interferometer configuration. The low pixel-pitch camera allows the digitizing of holograms with a higher spatial-frequency than what has been reported in the literature, allowing the recording of macroscopic objects closer to the camera sensor.

The reconstructed information can be visualized using 3D stereo glasses. From the perceived 3D we could identify several depth cues, including the occlusion effect which has not been easy to produce from single-aperture holography. The occlusion effect is also known to be difficult to produce from stereoscopic sources.

**Keywords:** Holography, Digital Holography, Angular Spectrum, Filtering, Stereo Image.

## 1. INTRODUCTION

High quality 3-D video is regarded by the general public as the ultimate viewing experience. The objective is well-understood and has been depicted in many popular fiction movies: the target is a magical and somewhat mysterious optical replica of an object that is visually indistinguishable from its original (except perhaps in size).<sup>1</sup>

Holography is a way to fully reconstruct a complex wavefield by recording its interference with a coherent reference beam. It was first presented by D. Gabor in 1948 while trying to improve electron microscopy.<sup>2</sup> With the invention of L.A.S.E.R., E. Leith and J. Upatnieks developed the first transmission hologram in 1962 while Y. Denisyuk developed the first reflection hologram. Traditionally, an hologram is an interference fringe that is recorded in photosensitive film using holography. When that pattern is illuminated with the reference light, the diffracted wavefield fully reconstructs the captured object along with all its properties: light intensity and depth; there is no optical difference between the real and reconstructed objects.

It wasn't much later that the first computer generated hologram (CGH) was produced, A. Lohmann and D. Paris made that breakthrough in 1967 using the limited computing capabilities at that time. In 1980 Yaroslavskii and Merzlyakov established the theoretical background for CGH. From here, holography turned into a important research topic and made its way into the most diverse applications including data storage, security, medical imaging, deformation/displacement measurement and of course, 3D displays.<sup>3,4</sup> Building digital holographic displays that are able to compete with current stereoscopic technology requires capabilities beyond actual electronic technology.<sup>3,4</sup>

The interference fringe - or hologram - can also be reconstructed numerically using a computer. First the hologram needs to be digitized using a digital camera; then wave propagation is simulated using the computer to produce the reconstructed object. To our knowledge L. Yu *et al.* were the first presenting a method for

---

Further author information: (Send correspondence to A.A.)

A.A.: E-mail: arrifano@i3s.unice.fr

M.A.: E-mail: am@i3s.unice.fr, Telephone: +33 492 942 718

P.T.F.: E-mail: fiadeiro@ubi.pt, Telephone: +351 275 319 703 / 746

M.P.: E-mail: mpereira@di.ubi.pt

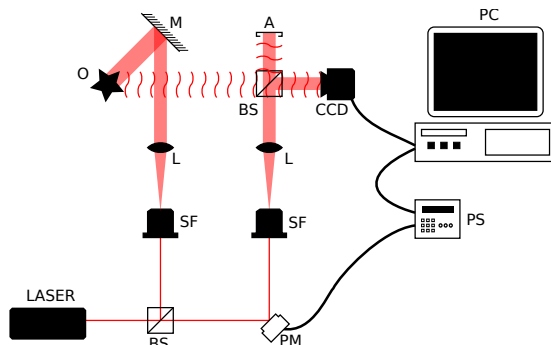


Figure 1. Holographic Recording Setup using a Mach-Zehnder configuration. A - light absorber; BS - beam-splitter; L - collimating lens; M - mirror; O - physical object; PM - piezo-electric mirror; PS - power supply; SF - spatial filter.

reconstruction of digital holograms with variable viewing angles.<sup>5</sup> They used a coordinate transformation in the Fresnel domain to account the new view, then the reconstructed complex amplitudes are numerically interpolated to compensate for the distortion caused by the changed coordinates. They experimentally demonstrate their method using digital holograms generated from 2D synthetic images. One year later, K. Matsushima presented a method<sup>6</sup> for the reconstruction of digital holograms in tilted planes. The method consists in wave propagation using the angular spectrum, where a rotation of the spectrum is performed using numerical interpolation. They demonstrate their method using simple diffraction patterns generated numerically. In 2008, T. Nakatsuji *et al.* presented a method for reconstruction of free-viewpoint images from synthetic aperture digital holograms.<sup>7</sup> In this method, the camera sensor is moved around in order to capture several holograms that, when tiled together, assemble a larger digital hologram. Then, waves are propagated from a sliding pupil in the hologram, using the angular spectrum; yielding to the reconstruction of several views. Three years later, in 2011, T. Pitkäaho *et al.* presented a method for calculating depth maps from digital holograms.<sup>8</sup> The method works by using the same pupil principle of Nakatsuji,<sup>7</sup> to produce a stereo pair. A depth map is then computed from the stereo pair using 3D image processing.

In this paper we present novel results on the reconstruction of stereo images from single (non synthetic-aperture) digital holograms recorded from real-world macroscopic objects. The method works by performing filtering in the angular spectrum of the object waves, which is computationally less expensive than the interpolation method of Matsushima.<sup>6</sup> If the complex amplitudes at the object plane are to be coded and stored (as suggested by some authors<sup>9</sup>) instead of the hologram transmittance, the presented method stands as a good alternative to the the sliding pupil method of Pitkäaho,<sup>8</sup> since it does not require wave-propagation.

In section 2 a description of the recording setup is made and the Fresnel Transform is briefly reviewed. Then in section 2.3 the proposed method is presented, followed by the experimental results (sec. 4) and conclusion (sec. 5).

## 2. DIGITAL RECORDING AND NUMERICAL RECONSTRUCTION OF HOLOGRAMS

### 2.1 The holographic acquisition system

The acquisition system (see fig. 1) follows a holographic interferometer configuration to produce in-line digital holograms. A beam-splitter is used to split a beam coming from a He-Ne 632.8 nm laser into the reference and object beams. The object beam is then spatially filtered using a microscope lens and pinhole, collimated and redirected to illuminate the object to be recorded. The reference beam hits a piezo-electric mirror, as done in<sup>10</sup> which allows shifting the phase electronically using the computer, providing phase-shifting holography.<sup>10</sup> The reference beam reflected from the mirror is then spatially filtered and collimated, resulting in a plane wave. The wavefront scattered from the object is superposed with the reference wavefront (fig. 1), resulting in an interference fringe. The fringe is then digitized by a Guppy F-503 camera, having a CMOS sensor with a  $2.2 \mu\text{m}$  pixel-pitch,  $2592 \times 1944$  pixels of resolution and 12bit bit-depth. This particular model was chosen due to its small pixel-pitch, compared to the  $6.8 \mu\text{m}$  which is the lowest we could find in the literature.<sup>11</sup>

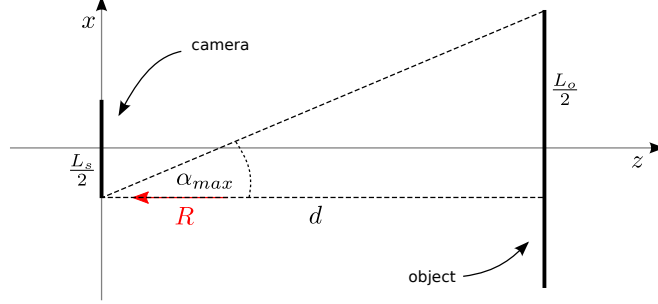


Figure 2. Hologram recording: maximum interference angle  $\alpha_{max}$  for in-line holography;<sup>12</sup>  $L_s$  and  $L_o$  are the lateral sizes of the camera sensor and object respectively,  $d$  is the recording distance.

The phase information of the wave superposition is naturally lost during the digitizing process, however by employing the phase-shifting technique<sup>10</sup> one can derive the complex amplitudes at the camera sensor plane (let us refer to them as the hologram transmittance  $\tau(x, y)$  from now on). By doing so, the numerical reconstruction also yields to holograms free of the zero-order and conjugate term.

## 2.2 The spatial frequency limitation

The maximum horizontal spatial frequency of an hologram at the camera plane is determined by its maximum interference angle  $\alpha_{max}$  (fig. 2) and the recording wavelength  $\lambda$ :

$$f_{max} = \frac{\sin(\alpha_{max})}{\lambda}. \quad (1)$$

Consider the experimental setup of fig. 2. The object is located at a distance  $d$  from the camera sensor and the reference wave  $R$  propagates normally to the sensor plane. The measures  $L_s$  and  $L_o$  are the lateral sizes of the sensor and object, respectively. If the sensor and object centres are assumed to be in the same optical path, the maximum interference angle is given by (fig. 2):

$$\alpha_{max} = \tan^{-1}\left(\frac{L_s + L_o}{2d}\right). \quad (2)$$

Ensuring that the sampling rate of the camera sensor is at least twice the maximum spatial frequency of the hologram yields to the recording of holograms free of aliasing:

$$f_{max} = \frac{1}{2\Delta x}. \quad (3)$$

In other words and considering the paraxial approximations, we can derive the following relationship from the previous equations:

$$\frac{1}{\Delta x} \geq \frac{L_s + L_o}{\lambda d}, \quad (4)$$

where  $\Delta x$  is the horizontal pixel-pitch of the camera sensor. Notice that a lower pixel-pitch camera sensor allows the recording of bigger objects and closer to the camera, providing a higher perception of depth.

## 2.3 Numerical reconstruction

Consider a plane wave  $R$  with wavelength  $\lambda$  diffracting on the hologram transmittance  $\tau(x, y)$ , producing the wavefield  $\Gamma$ . The object information can be numerically reconstructed at an plane  $\xi\eta$  parallel to the camera sensor and at an distance  $d$  from it, using the Fresnel transform:<sup>11</sup>

$$\begin{aligned} \Gamma(\xi, \eta) &= \frac{i}{\lambda d} e^{[-i2\pi/\lambda d]} e^{[-i\pi/\lambda d(\xi^2 + \eta^2)]} \\ &\times \int \int R(x, y) \tau(x, y) e^{[-i\pi/\lambda d(x^2 + y^2)]} \\ &\times e^{[i2\pi/\lambda d(\xi x + \eta y)]} dx dy. \end{aligned} \quad (5)$$

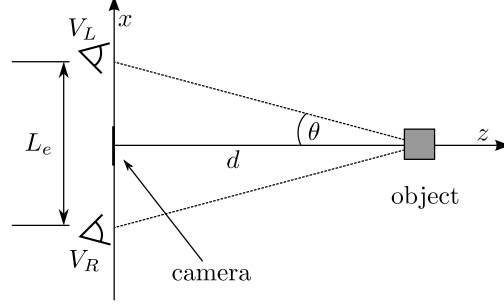


Figure 3. Geometry for the numerical reconstruction of the  $V_L, V_R$  stereo views.  $L_e$  is the average distance between eyes,  $d$  the recording distance.

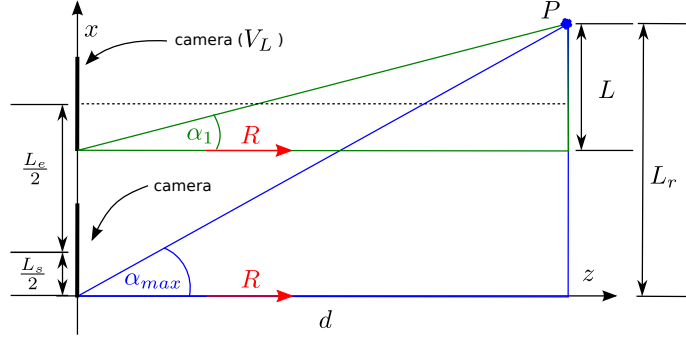


Figure 4. Highest angular frequency  $\alpha_{max}$  of the object spectrum, before and after a camera shift of  $L_e/2$ .

The reference wave  $R$  can be approximated by a complex amplitude with unitary amplitude and zero phase. Furthermore, eq. 5 can be easily discretized<sup>11</sup> and calculated using one FFT.<sup>13</sup>

The reconstructed intensities distribution of the object can then be obtained by:

$$I(\xi, \eta) = |\Gamma(\xi, \eta)|^2. \quad (6)$$

### 3. NUMERICAL RECONSTRUCTION OF A STEREO PAIR

#### 3.1 Introduction

Let us consider fig. 3, where the object lies at a distance  $d$  from the camera sensor. When the object is illuminated with coherent light some of the plane waves scattered from the object arrive into the camera sensor, interfering with the reference waves. The resulting interference fringe is digitized by the camera as the hologram transmittance  $\tau(x, y)$ . Then, as seen in the previous section, the diffracted field from the hologram transmittance is computed to produce the reconstructed image of the object.

Now imagine two apertures  $V_L, V_R$  providing a 3D stereo view of the object and placed at an distance  $L_e = 0.067$  m of each other, which is chosen to match the average interpupillary distance of a US male person.<sup>14</sup> By looking at figures 3, it is clear that each of the apertures allow plane waves with different directions to pass, corresponding to the information that would be visible by each of the views. In another words, each aperture behaves as a bandpass filter on the spatial frequency spectrum of the plane waves coming from the object, as explained in the next sections.

#### 3.2 The Angular Spectrum of the object waves

Let us reconsider the diffracted field  $\Gamma$  given by using the Fresnel Transform (eq. 5). The complex amplitudes  $\Gamma(\xi, \eta)$  are a superposition of plane waves with spatial frequencies  $f_x, f_y$ :

$$\Gamma(\xi, \eta) = \iint G(f_x, f_y) e^{j2\pi(f_x \xi + f_y \eta)}. \quad (7)$$

The inverse transformation also known as the angular spectrum (ASP) is given by:

$$G(f_x, f_y) = \iint \Gamma(\xi, \eta) e^{-j2\pi(f_x\xi + f_y\eta)}. \quad (8)$$

The spectrum  $G$  is bounded by  $[-f_{max}, f_{max}]$  in the  $x$ -axis, being  $f_{max}$  the maximum spatial frequency that the camera sensor can record (eq. 3).

### 3.3 Stereo views in the Angular Spectrum

Consider fig. 4 which depicts the highest angular frequency ( $\alpha_{max}$ ) of the object spectrum. Considering the paraxial case from now on,  $\alpha_{max}$  can be formulated as:

$$\alpha_{max} = \sin(\lambda f_{max}) \approx \lambda f_{max}. \quad (9)$$

The point  $P$  is the object point furthest away from the optical center in the  $x$ -axis, that can be recorded by the camera sensor. If there is a positive shift of  $\frac{L_e}{2}$  in the camera position (ending as view  $V_L$ ), then we can see that the corresponding angular frequency of point  $P$  is reduced to  $\alpha_1$ . With the help of fig. 4 we can then derive:

$$L_r = d \tan(\alpha_{max}) \approx d\alpha_{max}, \quad (10)$$

which allows us to calculate  $\alpha_1$ :

$$\alpha_1 = \frac{L_r - \frac{L_e}{2}}{d} = \frac{d\alpha_{max} - \frac{L_e}{2}}{d} = \alpha_{max} - \frac{L_e}{2d}. \quad (11)$$

One can also rewrite the previous equation as spatial frequencies:

$$f_1 = f_{max} - \frac{L_e}{2\lambda d}. \quad (12)$$

If we redraw fig. 4 to consider the lowest angular frequency instead, it is possible to formulate a similar expression:

$$f_2 = -f_{max} - \frac{L_e}{2\lambda d}. \quad (13)$$

The frequencies  $[f_2, f_1]$  are the new bounds of the object spectrum, visible at the view  $V_L$ . By looking closely at figure 4, we realize that the factor in equations 12 and 13:

$$f_s = \frac{L_e}{2\lambda d} \quad (14)$$

does actually represent a spatial-frequency shift in the object spectrum, caused by the displacement of the camera.

### 3.4 Filtering in the Angular Spectrum

As seen in the previous sections, the object spectrum  $G$  from eq. 8 is limited to  $[-f_{max}, f_{max}]$  in the  $x$ -axis (eq. 3). If moving the camera sensor about  $\pm L_e$  shifts the spectrum in about  $\pm f_s$  then it is clear that some frequencies get out of the spectrum while new frequencies come in. Those frequencies do actually correspond to the information that was only visible at each of the positions of the camera sensor. Because there is no way to know the new frequencies being shifted into the spectrum, we will consider them as zero. This way, an estimation of the spectrum corresponding to each view can be obtained by introducing a bandpass filter  $F_n$ :

$$\hat{G}(f_x, f_y) = F_n(f_x, f_y)G(f_x, f_y), \quad (15)$$

with  $n$  chosen to either  $L$  or  $R$ , according to the view that is being considered:

$$F_L(f_x, f_y) = \begin{cases} 1, & f_x \leq f_1 \\ 0, & f_x > f_1 \end{cases} \quad (16)$$

$$F_R(f_x, f_y) = \begin{cases} 1, & f_x \geq f_2 \\ 0, & f_x < f_2 \end{cases}. \quad (17)$$

An additional Fourier Transform must be performed (eq. 8) to get the filtered complex amplitudes  $\hat{\Gamma}(\xi, \eta)$  back. Each stereo view of the object can then be obtained by eq. using 6.

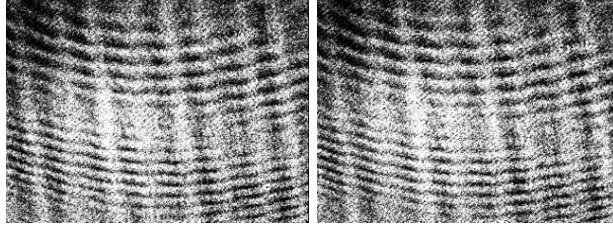


Figure 5. Scaled hologram transmittances for the "cube" (left) and "king" (right) objects. The visible fringes are low spatial frequencies and do not contribute significantly to the speckle noise of the reconstructed intensities.

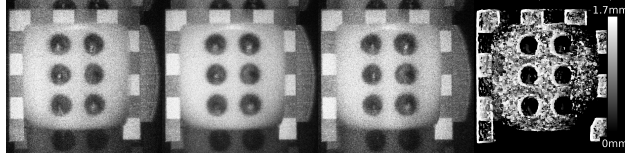


Figure 6. In order: Left, front, right, view reconstructions and disparity map of the "cube" hologram, scale 1:1 (1548 dpi).

#### 4. EXPERIMENTAL RESULTS

Consider the two hologram transmittances (fig. 5), obtained by using the the experimental setup described in section 2.1. The corresponding real-world objects were located at a distance  $d = 0.146$  m from the camera sensor, which is the lowest allowed by its spatial frequency limitation (see sec. 2.2).

The complex wavefield ( $\Gamma$ ) at the object plane is numerically reconstructed from a hologram transmittance by using the discrete Fresnel Transform (eq. 5). The calculation of the intensities distribution (eq. 6) from  $\Gamma$  leads to the front 2D view reconstruction of the object (figs. 6 and 7). To obtain a 3D stereo view reconstruction of the object, the ASP of  $\Gamma$  is calculated first. Afterwards, eq. 15 is evaluated for each of the views, the resulting filtered spectrums are then inverse Fourier transformed to produce  $\hat{\Gamma}_L, \hat{\Gamma}_R$ . The calculation of the intensities distribution (eq. 6) for each of the complex wavefields produces the left and right views of the object (figs. 6 and 7): the whole procedure is performed using 4 FFTs. Finally, to reduce the speckle noise, a temporarily incoherent illumination source is simulated.<sup>15</sup>

By visually comparing the L/R views from figs. 6 and 7 we could identify changes of lightening and a subtle occlusion effect, due to the change of viewpoint. Binocular disparity (calculated using the method from<sup>8</sup>) is also present as seen in the same figures. We were also able to perceive depth using the NVIDIA 3D vision<sup>®</sup> active shutter glasses, despite the speckle nature of the images.

It is interesting to point out that after filtering in the ASP of the object, the bandwidth left for reconstruction was only 20%. Nonetheless, it does not seem to cause significant degradation in the speckle quality of the reconstruction. Also, the "ghosting" effects visible in both reconstructions are not aliasing effects, being just reflections of the object inside the beam-splitter surfaces (fig. 1). Finally, the images displayed in this paper (figs. 6 and 7) had their luminance equalized to increase perceptibility when printed, this has the side effect of increasing the speckle noise as well.

#### 5. CONCLUSION

We were successful at the numerical reconstruction of a stereo pair from a single digital hologram. The reconstructed information can be visualized using 3D stereo glasses, providing the sensation of stereopsis. From the

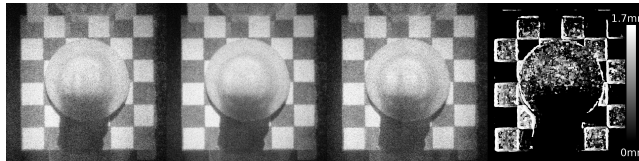


Figure 7. In order: Left, front, right, view reconstructions and disparity map of the "king" hologram, scale 1:1 (1548 dpi).

perceived 3D we could identify several depth cues, including the occlusion effect.

If the complex amplitudes at the object plane are to be coded and stored instead of the hologram transmittance, the presented method stands as a good alternative to the the sliding pupil method of,<sup>8</sup> since it does not require wave-propagation.

With the upcoming 4k digital format it is expected that new higher-resolution cameras will be available, allowing the reconstruction of more than two views using the presented method.

## ACKNOWLEDGMENTS

The author Angelo Arrifano thanks Fundação para a Ciência e Tecnologia (FCT) for his PhD grant with reference number SFRH/BD/69710/2010.

## REFERENCES

- [1] Onural, L., “Television in 3-D: What are the prospects?,” *Proceedings of the IEEE* **95**(6), 1143–1145 (2007).
- [2] Gabor, D., “Microscopy by reconstructed wave-fronts,” *Proceedings of the Royal Society of London A* **197**(1051), 454–487 (1949).
- [3] Onural, L., Yaraş, F., and Kang, H., “Digital holographic three-dimensional video displays,” *Proceedings of the IEEE* **99**(4), 576–589 (2011).
- [4] Yaras, F., Kang, H., and Onural, L., “State of the Art in Holographic Displays: A Survey,” *Journal of Display Technology* **6**(10), 443–454 (2010).
- [5] Yu, L., An, Y., and Cai, L., “Numerical reconstruction of digital holograms with variable viewing angles,” *Optics Express* **10**, 1250–7 (Nov. 2002).
- [6] Matsushima, K., Schimmel, H., and Wyrowski, F., “Fast calculation method for optical diffraction on tilted planes by use of the angular spectrum of plane waves,” *Optical Society of America A* **20**, 1755–62 (Sept. 2003).
- [7] Nakatsuji, T. and Matsushima, K., “Free-viewpoint images captured using phase-shifting synthetic aperture digital holography,” *Applied Optics* **47**, D136–43 (July 2008).
- [8] Pitkäaho, T. and Naughton, T. J., “Calculating depth maps from digital holograms using stereo disparity,” *Optics Letters* **36**, 2035–7 (June 2011).
- [9] Darakis, E., Naughton, T. J., and Soraghan, J. J., “Compression defects in different reconstructions from phase-shifting digital holographic data,” *Applied Optics* **46**, 4579–86 (July 2007).
- [10] Yamaguchi, I. and Zhang, T., “Phase-shifting digital holography,” *Optics Letters* **22**, 1268–70 (Aug. 1997).
- [11] Schnars, U. and Jüptner, W., “Digital recording and numerical reconstruction of holograms,” *Measurement Science and Technology* **13**, 4812–20 (Aug. 2002).
- [12] Xu, L., “Properties of digital holography based on in-line configuration,” *Optical Engineering* **39**(12), 3214–3219 (2000).
- [13] Schnars, U. and Jüptner, W., “Direct recording of holograms by a CCD target and numerical reconstruction,” *Applied Optics* **33**, 179–81 (Jan. 1994).
- [14] Dodgson, N., “Variation and extrema of human interpupillary distance,” *SPIE Proceedings Electronic Imaging* **5291**, 36–46 (2004).
- [15] Hennelly, B. M., Kelly, D. P., Maycock, J., Naughton, T. J., and McDonald, J., “Speckle Reduction from Digital Holograms by Simulating Temporal Incoherence,” *Proceedings of the SPIE* **6696**, 66961I–12 (2007).